Journal of Environmental Chemical Engineering 8 (2020) 103922

Contents lists available at ScienceDirect

Journal of Environmental Chemical Engineering

journal homepage: www.elsevier.com/locate/jece

Synthesis and physicochemical characterization of a novel adsorbent based on yttrium silicate: A potential material for removal of lead and cadmium from aqueous media

Vinicius Litrenta Medeiros[a], Leandro Goulart de Araujo[b], Davi Rubinho Ratero[a], Alex Silva Paula[a], Eduardo Ferreira Molina[c], Christian Jaeger[d], Júlio Takehiro Marumo[b], José Geraldo Nery[a,*]

[a] Department of Physics, Institute of Biosciences, Letters and Exact Sciences, São Paulo State University (UNESP), Campus of São José Do Rio Preto, SP, 15054-000, Brazil
[b] Nuclear and Energy Research Institute (IPEN), Av. Prof. Lineu Prestes 2242, São Paulo, SP, 05508-000, Brazil
[c] University of Franca, Av. Dr. Armando Salles Oliveira 201, Franca, SP, 14404-600, Brazil
[d] BAM - Federal Institute for Materials Research and Testing, Division 1.3 Structure Analysis, NMR Spectroscopy, 12489 Berlin, Germany

ARTICLE INFO

Editor: Yunho Lee

Keywords:
Yttrium silicates
^{29}Si
^{89}Y MAS-NMR
Adsorption
Chemisorption
Cadmium and lead remediation

ABSTRACT

A new metallosilicate based on yttrium was synthesized and characterized by XRD, FT-IR, ^{29}Si MAS-NMR, and ^{89}Y MAS-NMR. The mixed framework of the material was confirmed by the detection of distinct chemical shift groups using ^{29}Si MAS-NMR (at -82 to -87 ppm, -91 to -94 ppm, -96 to -102 ppm, and -105 to -108 ppm), as well as four distinct chemical shifts in the ^{89}Y MAS-NMR spectrum (at -89, -142, -160, and -220 ppm). Adsorption and kinetic analyses indicated the potential of the new material for the removal of lead and cadmium from aqueous media. The adsorption results for lead indicated that dynamic equilibrium was reached after five hours, with total lead removal of around 94 %, while for cadmium it was reached in the first hour, with total cadmium removal of around 74 %. The adsorptions of lead and cadmium were modeled using pseudo-first order (PFO) and pseudo-second order (PSO) kinetic models. Although both models provided high R^2 values (0.9903 and 0.9980, respectively), the PSO model presented a much lower χ^2_{red} value ($4.41 \times 10-4$), compared to the PFO model ($2.12 \times 10-3$), which indicated that the rate-limiting step was probably due to the chemisorption of lead from the solution onto the yttrium-based metallosilicate.

1. Introduction

Heavy metals such as lead and cadmium are released from a wide range of anthropogenic activities, reaching aquatic environments where their presence can affect the biota and cause health problems in humans. Therefore, the removal of heavy metal pollutants from aqueous systems has received a considerable amount of attention. Lead (Pb^{2+}) is highly toxic and dangerous, since it can enter the body by the respiratory route or in food, subsequently accumulating and persisting in the organism for several years. Health effects associated with Pb^{2+} poisoning include cancer, DNA mutations, behavioral alterations (especially in children), liver problems, reproductive system dysfunction, and brain disorders, among others [1,2]. Contamination of the environment by Pb^{2+} is mainly associated with anthropic sources such as mining, smelting, car emissions, use of pesticides, irrigation with contaminated water, and improper disposal of industrial waste [3].

Cadmium (Cd^{2+}) can also cause serious harm to the environment and human health, due to its toxic properties. The metal can accumulate in the bloodstream over long periods of time, causing poisoning and death by reducing calcium (Ca^{2+}) in the bones, leading to the development of osteomalacia and osteoporosis [4,5]. In previous studies, Pb^{2+} and Cd^{2+} have been removed from contaminated soils and aqueous media using different types of adsorbents [6,7] including fly ash [8], Composites [9], kaolinite clay [10], biomass [11], red mud [12], microorganisms [13,14], natural zeolites, and other low cost adsorbents [15,16].

Zeolites are crystalline microporous materials, based on aluminosilicates, with well-defined pore structures built of $[SiO_4]^{4-}$ and $[AlO_4]^{5-}$ tetrahedra, generally with diameters smaller than 10 Å and containing active sites that can be generated in the zeolite framework [17]. Depending of the zeolites chemical composition, different pore sizes, acidity, basicity, thermal resistance, and selectivity ion exchange,

* Corresponding author at: Department of Physics, São Paulo State University (UNESP), Campus of São José do Rio Preto, SP, 15054-000, Brazil.
E-mail address: geraldo.nery@unesp.br (J.G. Nery).

https://doi.org/10.1016/j.jece.2020.103922
Received 20 November 2019; Received in revised form 16 March 2020; Accepted 30 March 2020
Available online 07 April 2020

as well as different specificities of the active catalytic sites can be formed. These properties have direct dependence on the conditions of the synthesis and the way that it is performed. The materials are usually synthesized by hydrothermal sol-gel reactions, under specific conditions of temperature and pressure, with the pH controlled to fine-tune the final properties of the silicates. The strength and concentration of the active sites, surface area, and the adsorption properties can be tailored for specific applications, particularly in catalysis and for environmental remediation [18–21]. The substitution of Si or Al atoms of the zeolite crystallographic network by other transition metals (such as Ti, V, Zr, Ge, Nb, Y, Cr, and Mo) results in zeolites with different physicochemical characteristics, including porosity, channel, and cavity topologies [22].

Among the microporous materials with mixed frameworks, titanosilicates such as ETS-10 and ETS-4 have been widely employed in heavy metal removal [23–25]. In contrast, natural yttrium silicates have been studied in terms of their structural and physicochemical properties, but there has been little systematic investigation of their potential as adsorbents for environmental remediation. Concerning this application, few works have been mentioned about minerals with both tetrahedral silicon and octahedral yttrium spirals include sazykinaite ($Na_5YZrSi_6O_{18}.6H_2O$) [26], pyatenkoite ($Na_5YTiSi_6O_{18}.6H_2O$) [27], monteregianite ($Na_4K_2Y_2Si_{16}O_{38}.10H_2O$) [28], and synthetic yttrium silicates include AV-1 [22], (Rb, Cs)$_9Y_7Si_{24}O_{63}$, $Rb_9Y_7Si_{24}O_{63}$, Ba-$KYSi_2O_7$, and $Cs_3YSi_8O_{19}$ [29,30].

In this work, a novel yttrium silicate was synthesized in a facile and straightforward method and fully characterized by XRD, FT-IR, BET, ^{29}Si MAS-NMR, ^{89}Y MAS-NMR and its adsorption proprieties were also studied for the removal of Pb^{2+} and Cd^{2+} of ions from aqueous medium.

2. Experimental

2.1. Yttrium silicate synthesis

The source of yttrium used in this work was YPO_4 (Aldrich). NaOH (Merck) and KOH (Synth) were used as alkaline agents. The silicon source was Ludox HS-30 sodium silicate solution (27 % w/w SiO_2, Aldrich). NaCl (Aldrich) was used as a stabilizing agent. The material was synthesized using 1.05 g YPO_4, 0.24 g KOH, 0.39 g NaOH, 0.23 g NaCl, 18.91 g H_2O, and 5.19 g Ludox HS-30. First, a solution (solution A) was prepared by mixing together 10 g of H_2O, 0.24 g of KOH, and 0.39 g of NaOH, under magnetic stirrer until complete dissolution. Ludox HS-30 (5.19 g) and NaCl (0.23 g) were then added to solution A, under constant stirring until the NaCl crystals had completely dissolved. Another solution (solution B) was prepared with 8.91 g of H_2O and 1.05 g of YPO_4, under constant stirring until the phosphate was solubilized. The last step was to mix the two solutions, followed by stirring for 1 h, at room temperature. The final pH of the mixture (solution A + B) was ~13 and the resulting gel showed a white color. At the end of this step, the gel was transferred to a Teflon jacket, which was placed in an autoclave reactor and heated in an oven (model 315 SE, FANEM, Brazil) for 6 days at 230 °C. The resulting solid was washed and filtered, at room temperature, using deionized water, followed by drying in an oven at 60 °C for 12 h. The as-synthesized material was denoted MYS (Metallo-Yttrium Silicate).

2.2. Adsorption experiments

Cadmium and lead solutions were prepared by dissolving cadmium chloride $CdCl_2$ and lead(II) nitrate $Pb(NO_3)_2$ (Merck, Brazil) in distilled water. Both solutions were prepared at concentration of 0.05 and 0.1 mol L^{-1}. The initial pH values of the prepared salts solutions were 1.74 ($CdCl_2$) and 3.70 ($Pb(NO_3)_2$), while typical pH value for the yttrium silicate in aqueous medium (0.5 g/ 15 mL) was around pH = 9.7. No pH adjustments were carried out at the beginning or during the Kinect studies. Kinetic adsorption assays were performed using a batch system. All the experiments were performed in duplicate. For this purpose, 0.5 g of the MYS was placed in contact with 15 ml of salt solution. The mixture was shaken in an orbital shaker (model BT 400, Biothec, Brazil), at 120 rpm and 22 − 23 °C. The contact times employed were 30, 60, 120, and 240 min (for [$CdCl_2$ or $Pb(NO_3)_2$]$_0$ = 0.10 mol L^{-1}), and 60, 120, 240, 300, 360, 420, and 480 min (for [$CdCl_2$ or $Pb(NO_3)_2$]$_0$ = 0.05 mol L^{-1}). The ion-exchanged MYS was separated by filtration using filter paper (slow filtration for fine precipitates, 3 µm pore size), with ash content of 0.00012 g (Millipore, USA), employing a vacuum system. The ion-exchanged materials were denoted MYS/Cd and MYS/Pb. The filtrate was collected and reserved for subsequent determination of the concentrations of Pb^{2+} and Cd^{2+} ions by inductively coupled plasma optical emission spectroscopy (ICP-OES, model Optima 7000DV, PerkinElmer, USA). The samples were prepared separately for each contact time, using the same initial metal concentration.

2.3. Physicochemical characterization

Powder X-ray diffraction (XRD) analyses were performed using a Rigaku Miniflex II diffractometer operating at 30 kV and 15 mA, with a nickel filter and Cu Kα radiation (λ = 1.5418 Å). The diffraction patterns were obtained in the 2θ range from 3° to 60°, at a scan rate of 2° (2θ) min^{-1}. For step-scan analysis, the scan rate was 0.1° (2θ) min^{-1}. Scanning electron microscopy (SEM) images were recorded at the Brazilian National Nanotechnology Laboratory (National Center for Energy and Materials Research), in Campinas (São Paulo State), using a Phillips XL30 FEG instrument operating with electron beam voltages from 5 to 25 kV. Additional analyses were performed at LCE-DEMa (UFSCar, São Carlos, São Paulo State), using an FEI Inspect S50 scanning electron microscope operated with an electron beam voltage of 25 kV.

Fourier transform infrared spectroscopy (FT-IR) analyses were performed using a spectrometer (model Frontier, PerkinElmer, USA) equipped with an ATR germanium crystal. The spectrum was analyzed in the region from 600 to 4000 cm^{-1}. The concentrations of cadmium and lead were determined by ICP-OES (Optima 7000DV, PerkinElmer, USA). Calibration solutions were prepared by dilution of certified cadmium and lead standard solutions (Johnson Matthey, UK). The wavelengths (λ) used were 228.802 nm (cadmium) and 220.353 nm (lead). The plasma views were radial (cadmium) and axial (lead). The results were expressed as the average of duplicate measurements. The textural properties of the solid samples were analyzed at −196 °C, using an adsorption analyzer (ASAP 2020, Micromeritics). For this purpose, ~0.2 g of the sample was degassed at 150 °C, for 24 h, and the specific surface area was obtained by the BET method. The total pore volume was calculated according to the amount of adsorbed N_2.

2.4. ^{29}Si MAS-NMR and ^{89}Y MAS-NMR

The ^{29}Si MAS-NMR experiments were performed using a two-channel spectrometer (Avance III 400 MHz, Bruker) equipped with a 7 mm (low gamma) probe. The spectra were obtained at 79.5 MHz, in a 9.4 T magnetic field, at room temperature, using 90° pulses of 4 µs duration, with 10 s delay, 4096 scans, 32 kHz spectrum length, and 4096 points. The chemical shifts were obtained using a kaolin standard at −91.1 ppm. A sample of YF_3 was used to obtain the ^{89}Y spectrum, applying a 90° pulse of 10.5 µs duration.

Chemical shifts were referenced to the YF_3 resonance centered at −108.7 ppm. Magic angle spinning (MAS) experiments were performed with a rotation speed of 5 kHz, with no need for hydrogen decoupling, because heteronuclear dipole coupling was insignificant, due to the large inter-nuclear distance between the ^{89}Y and ^{1}H atoms, together with a small ^{89}Y ratio. For the MYS sample, three spectra were acquired and summed, with repetition times and averages, respectively, of 120 s

and 1280, 240 s and 1280, and 30 s and 1782. For the MYS/Cd sample, a measurement was performed with repetition time of 120 s and average of 2650. For MYS/Pb, two spectra were acquired and summed, with repetition times and averages, respectively, of 240 s and 2560, and 120 s and 2560.

2.5. Data evaluation

The uptakes of cadmium and lead by the MYS in the batch adsorption experiments were determined using the following equation:

$$Q = (C_o - C)\frac{V}{m} \quad (1)$$

where Q is the uptake of the metal (mmol. g^{-1}), C_o is the initial metal concentration in solution (mmol.L^{-1}), C is the equilibrium concentration in solution (mmol.L^{-1}), V is the solution volume (L), and m is the MYS mass (g)."

2.6. Kinetic data

The adsorption of Pb^{2+} on the MYS was modeled using pseudo-first order (PFO) and pseudo-second order (PSO) kinetic models. The PFO model [31] is given by:

$$q_t = q_e[1 - \exp(-k_1 t)] \quad (2)$$

where q_t and q_e are the amounts of solute (mmol) adsorbed per gram of adsorbent at any time and at equilibrium, respectively, and k_1 (min^{-1}) is the PFO rate constant. The PSO model [32] is given by:

$$q_t = \frac{k_2 q_e^2 t}{1 + k_2 q_e t} \quad (3)$$

where k_2 (g. $mmol^{-1}$. min^{-1}) is the PSO rate constant.

2.7. Error evaluation

The batch experimental adsorption data were modeled by nonlinear regression analysis, using Origin Pro ® 9.1 software with the kinetic models. The Levenberg-Marquardt iteration algorithm and weighted nonlinear regression were employed, with reduced chi-square (χ^2_{red}) as the objective function [33].

3. Results and discussion

The XRD pattern of the as-synthesized MYS material is shown in Fig. 1. A careful comparison was made of the diffraction peaks observed for MYS and for other natural yttrium silicates reported in the literature, including sazykinaite [26], pyatenkoite [27], and monteregianite [28], as well as synthetic materials such as AV-1 [22], and a different XRD pattern were assigned (Fig.1 red arrows). Indexation of the main diffraction peaks, using TREOR software [34], resulted in a monoclinic unit cell (a = 13.26 Å; b = 9.25 Å; c = 12.37 Å; α = 90°; γ = 90°; β = 114.76°). The unit cell was similar to the one reported by Ghose et al. [28] for the natural yttrium silicate monteregianite, which also has a monoclinic unit cell (a = 9.512 Å; b = 23.956 Å; c = 9.617 Å; α = 90°; γ = 90°; β = 93.85°). According to the crystallographic structure reported by Ghose et al. [28], the crystal structure of monteregianite consists of two different types of layers alternating along the [010] direction: (a) a double silicate sheet, where the single silicate sheet is of the apophyllite type, with four- and eight-membered rings, and (b) an open octahedral sheet composed of [YO_6] and three distinct [$NaO_4(H_2O)_2$] octahedra. The layers are parallel to the (010) plane. The K atoms are ten-coordinate and the six water molecules are located within large channels formed by the planar eight-membered silicate rings. In principle, sodium and potassium can be replaced by other alkali metals using ion exchange procedures, under appropriate experimental conditions. In order to investigate this possibility, ion exchange experiments with lead (Pb^{2+}) and cadmium (Cd^{2+}) were conducted with the as-synthesized MYS materials, according to the experimental conditions described in Section 2.2. The effects of the ion replacements on the original crystallographic structure of the as-synthesized material are shown in Fig. 2.

The XRD patterns for MYS/Pb and MYS/Cd showed that the ion exchange drastically changed the original structure. In the case of MYS/Pb, it can be observed that peaks originally present in the as made MYS at 2θ = 12.60, 14.30, 16.01, 20.07, 23.67, 28.85, 32.30, 34.90, 42.04, and 51.70° were absent (Fig. 2, absent diffraction peaks highlighted in blue arrows). Meanwhile for MYS/Cd, the main absent diffraction peaks were the ones originally present at 2θ = 12.60, 14.30, 16.02, 23.96, 28.89, 29.90, and 33.72° (Fig. 2, absent diffraction peaks highlighted in red arrows). The drastic changes observed in the XRD patterns of MYS after ion exchange suggest that the presence of these species modified the MYS structure evidencing a high affinity of the material for Pb^{2+} and Cd^{2+}.

The effect of the ion exchange on the morphology of the as-synthesized MYS was investigated by SEM analysis (Fig. 3). The as-synthesized MYS is formed by well-defined crystal platelets around 10 − 50 μm in size (Fig. 3a,b) typical of layered materials. After the ion exchange, MYS/Pb and MYS/Cd (Fig. 3c and d) derivatives still retained some of the original morphology, although it could be seen that the ion exchange led to the formation of debris fibers on the surfaces of the crystals.

The FT-IR spectra of the as-synthesized MYS material and the ion-

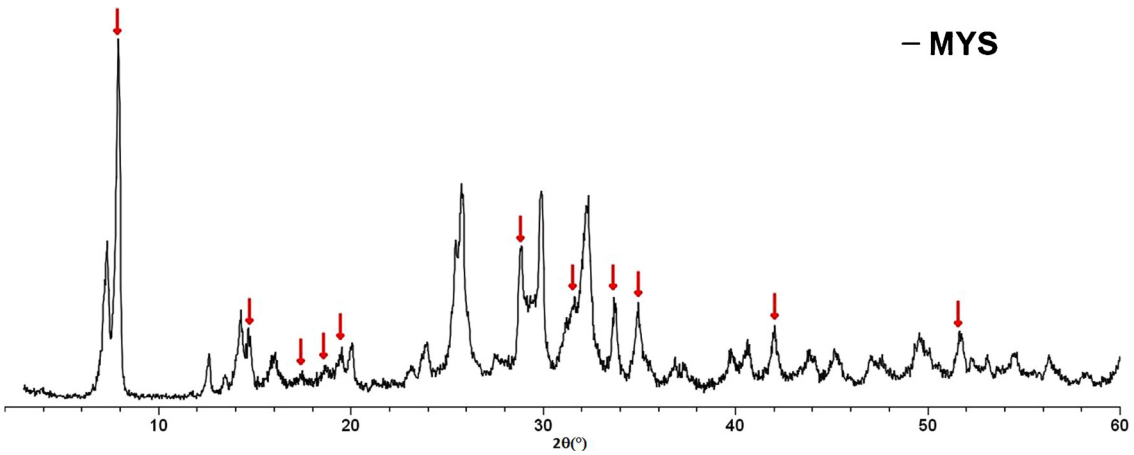

Fig. 1. XRD pattern of the as made yttrium silicate material (MYS). The arrows indicate the new diffraction peaks present only in the MYS material in comparison with other yttrium silicate reported in the literature [28–30].

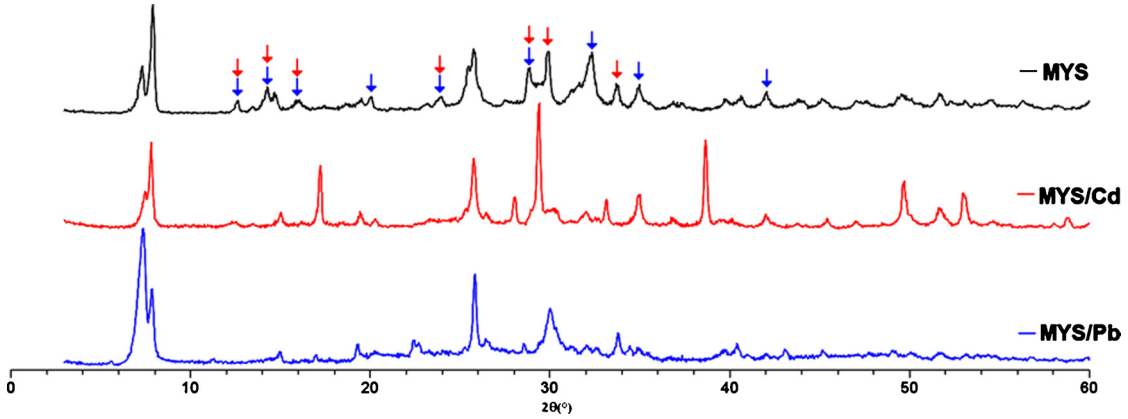

Fig. 2. XRD patterns of the as made yttrium silicate (MYS) and its cadmium (MYS/Cd) and Lead (MYS/Pb) derivates. The arrows highlight the absent diffraction peaks originally present in MYS material.

exchanged MSY/Pb and MYS/Cd derivatives are shown in Fig. 4. MYS, MYS/Pb, and MYS/Cd showed absorption bands at 3448, 3622, 1634, 1200, 1000, 994, 781, 692, 515, and 455 cm^{-1}. The absorption bands located in the 3400 − 3600 cm^{-1} region were mainly associated with the silanol groups Si − OH. The bands at 1172, 1028, and 935 cm^{-1} were associated with asymmetric stretches of the framework atoms, while the bands at 755, 690, and 610 cm^{-1} corresponded to symmetric stretches. The 450 cm^{-1} absorption band could be attributed to bending vibration at the Si(4Si) sites in the SiO_4 tetrahedron [22] The most relevant difference was observed for MYS/Pb, for which an absorption band at 1383 cm^{-1} which could attributed to the formation of lead oxide hydroxide clusters such $[Pb_3(OH)_4]^{2+}$, and $[Pb_4(OH)_4]^{4+}$ as commonly found in the zeolite cavities [35–39]. The FTIR differences between MYS and MYS/Pb could be related with the high adsorbed amount of Pb^{2+} ions (see Fig. 11) by the materials. The MYS/Pb and MYS/Cd materials showed decreased intensities of the adsorption bands at 935 and 450 cm^{-1} compared to the as-synthesized MYS, which reflected the modification associated with asymmetric stretches and bending vibration between atoms of the SiO_4 tetrahedron of the yttrium silicate framework. Briefly, the experimental evidences provided by FT-IR, XRD and SEM data corroborate the drastic structural changes of the original yttrium silicate caused by the Pb and Cd ions adsorption

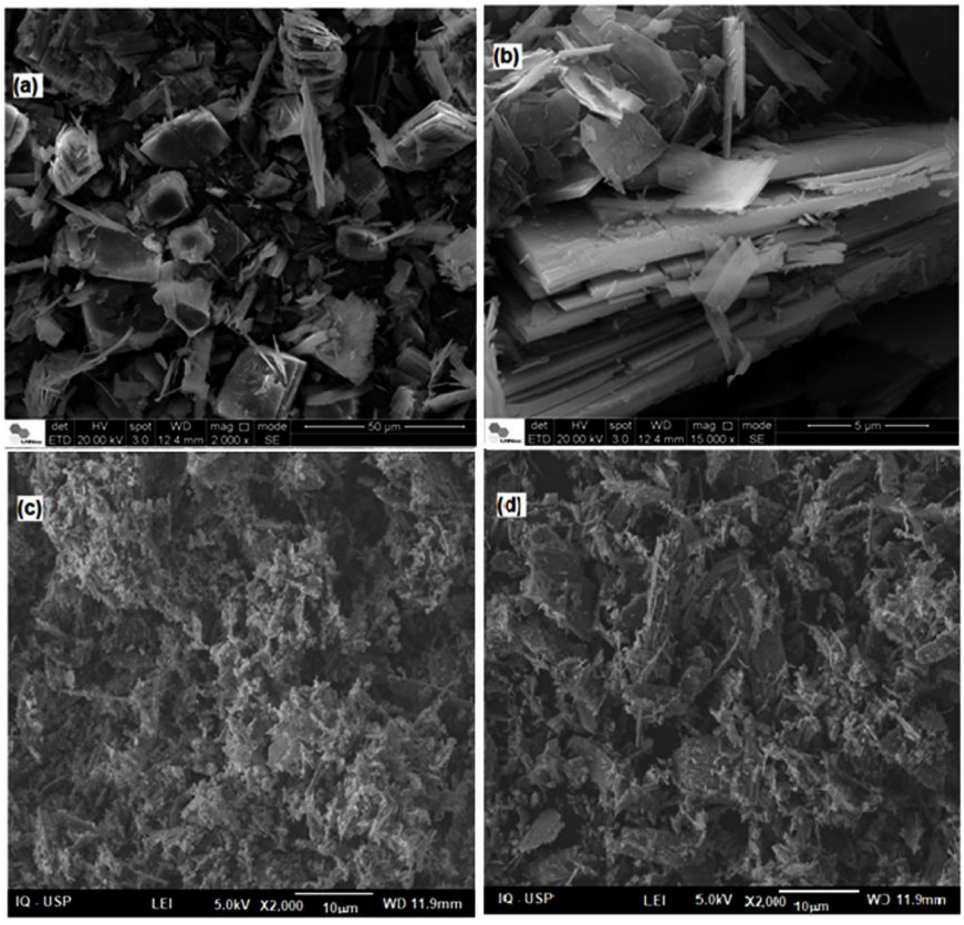

Fig. 3. SEM images of (a, b) the as-synthesized MYS, (c) MYS/Pb, and (d) MYS/Cd.

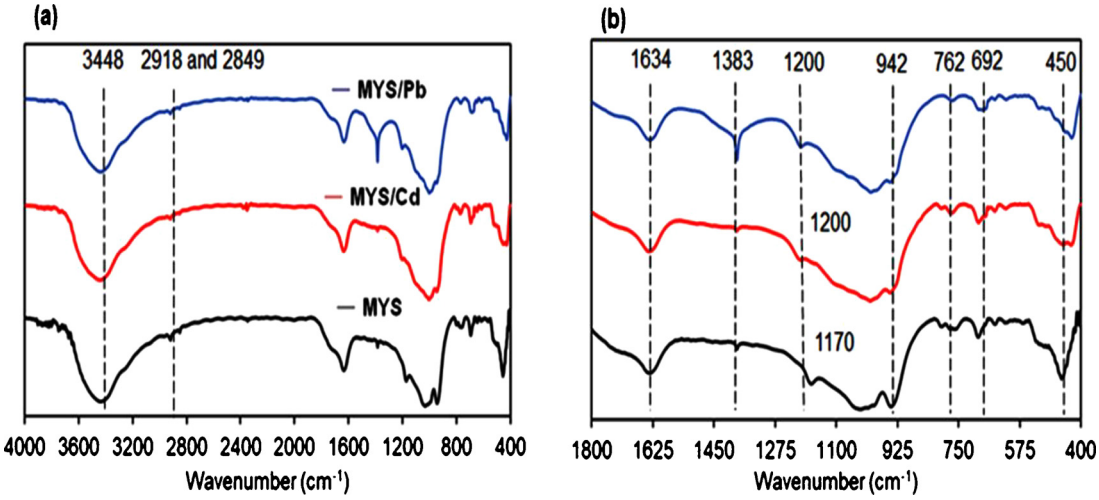

Fig. 4. (a) FT-IR spectra of MYS (black line), MYS/Cd (red line), and MYS/Pb (blue line), in the region 400-4000 cm^{-1}. (b) Magnification of the bands in the region 400-1800 cm^{-1}.

experiments.

The porosities of the as-synthesized MYS and the ion-exchanged derivatives (MYS/Pb and MYS/Cd) were investigated using N_2 adsorption/desorption experiments (Fig. 5, Table 1). All the materials presented type II isotherms with H3 hysteresis, indicating the presence of macropores. According to the IUPAC classification, a hysteresis loop between the adsorption and desorption branches is characteristic of macroporous materials. The calculated surface areas of 3.0, 2.8, and 19.0 $m^2 g^{-1}$ for MYS, MYS/Pb, and MYS/Cd, respectively, were in good agreement with the values reported for other synthetic yttrium silicates.

Table 1
Porous characteristics of the pristine yttrium silicate and the materials after adsorption of the cations.

Material	BET surface area ($m^2 g^{-1}$)	Total pore volume ($cm^3 g^{-1}$)	Pore width (nm)
MYS	3.00 ± 1	0.054 ± 0.01	70.0
MYS-Cd	19.0 ± 1	0.097 ± 0.01	20.0
MYS-Pb	2.80 ± 1	0.084 ± 0.01	121.5

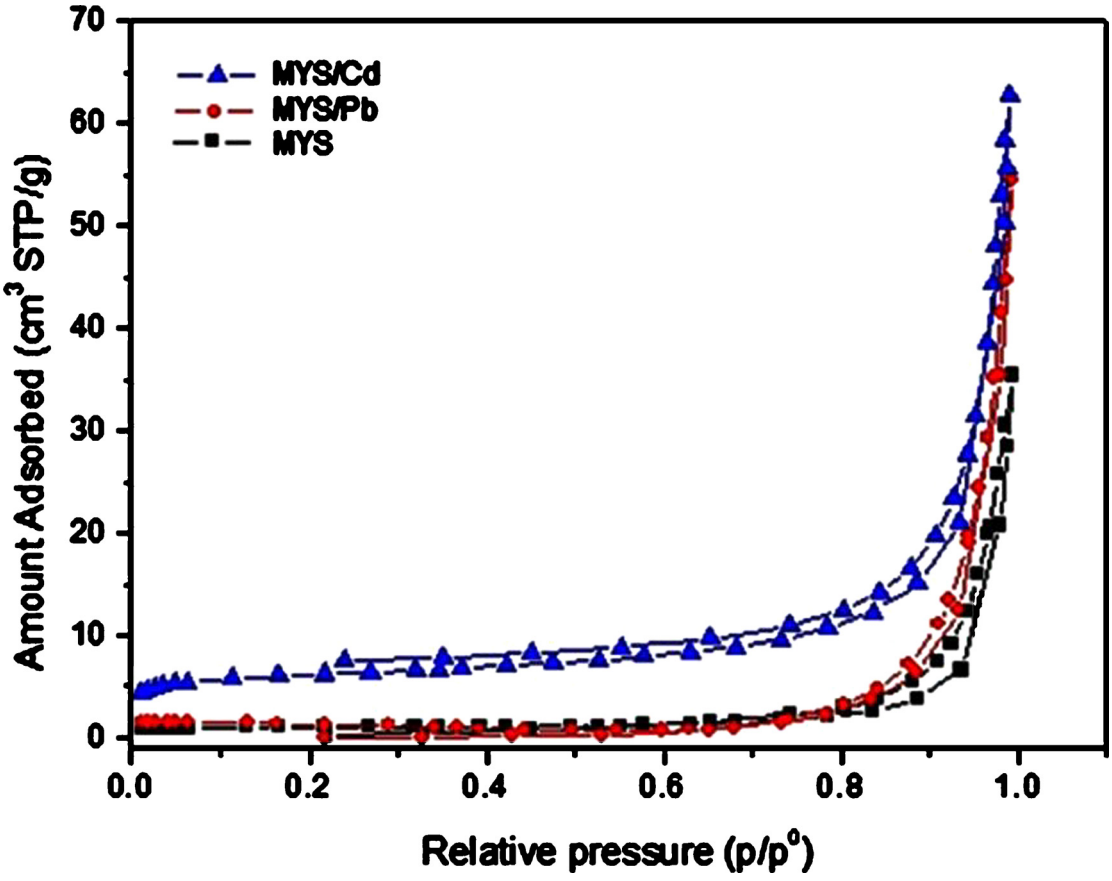

Fig. 5. Nitrogen adsorption-desorption isotherms for the pristine yttrium silicate and the materials after adsorption of Pb^{2+} and Cd^{2+} cations.

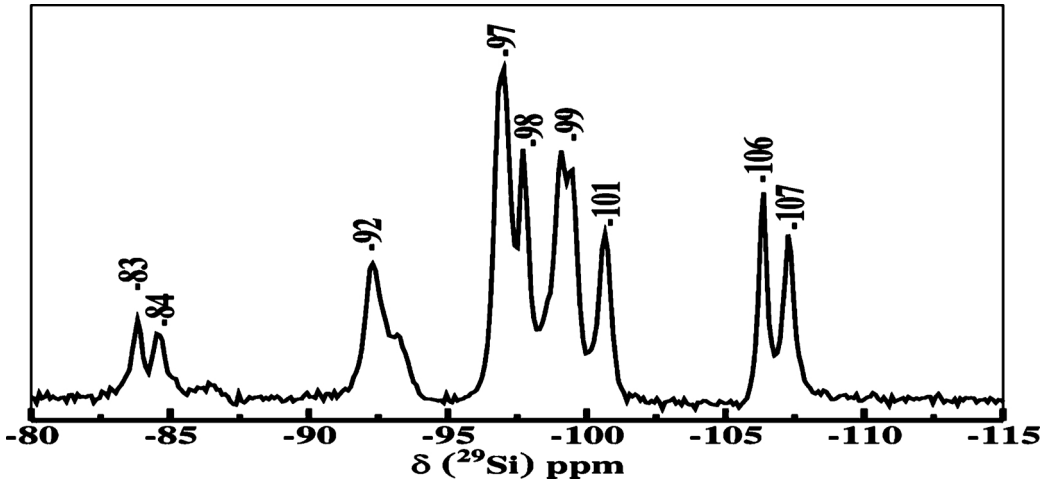

Fig. 6. ^{29}Si MAS-NMR spectrum of the as-synthesized metallo-yttrium silicate (MYS).

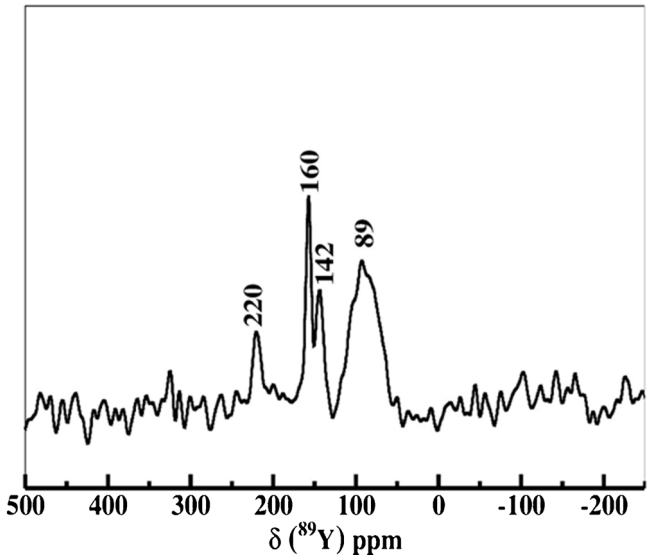

Fig. 7. ^{89}Y MAS-NMR spectrum of the as-synthesized metallo-yttrium silicate (MYS).

The ^{29}Si MAS-NMR spectrum for the MYS material (Fig. 6) showed four groups of resonances, in the ranges -82 to -87 ppm, -91 to -94 ppm, -96 to -102 ppm, and -105 to -108 ppm. The chemical environment observed for MYS was quite different from the one reported previously for the AV-1 yttrium silicate, which presented only two resonance groups, in the ranges -96 to -102 ppm and-105 to -108 ppm [40,41]. Therefore, the presence of the two extra resonance groups with chemical shifts in the ranges -82 to -87 ppm and-91 to -94 ppm, observed for MYS, corroborated the XRD data indicating that MYS was an yttrium silicate with a crystallographic structure different from those reported previously. The assignments of the MYS chemical shifts were performed considering the well-known correlation between the ^{29}Si chemical shifts and the Si-O bond lengths in silicates.

The chemical shifts at -105 and -108 ppm could be assigned to Si (4Si) sites, corresponding to a chemical environment with one Si atom linked to four other Si atoms by oxygen bridges. Based on the results reported by Rocha et al. [22] for the AV-1 yttrium silicate, it was reasonable to assign the chemical shift at -102 ppm to the Si(3Si, 1Y) site. The assignment of the other peaks at high frequency was more difficult, because MYS has more distinct Si sites, compared to AV-1, as clearly shown by the ^{29}Si MAS-NMR spectra [22].

The ^{89}Y MAS-NMR spectrum of the as-synthesized MYS presented four chemical shifts, at -89, -142, -160, and -220 ppm (Fig. 7). It should be noted that, to the best of our knowledge, there is no report in the literature describing the ^{89}Y MAS-NMR spectra for monteregianite and the AV-1 yttrium silicate. According to the crystallographic structure of monteregianite, there is only one octahedral coordinated yttrium site (YO_6) [42], which could be assigned to the chemical shift at -89 ppm. However, correct assignment of the signals at -142, -160, and -220 ppm is not straightforward without knowledge of the crystallographic structure of MYS. Nevertheless, the chemical shifts at -142, -160, and -220 ppm could be related to yttrium species that did not have octahedral coordination, since the chemical shift increases as the yttrium

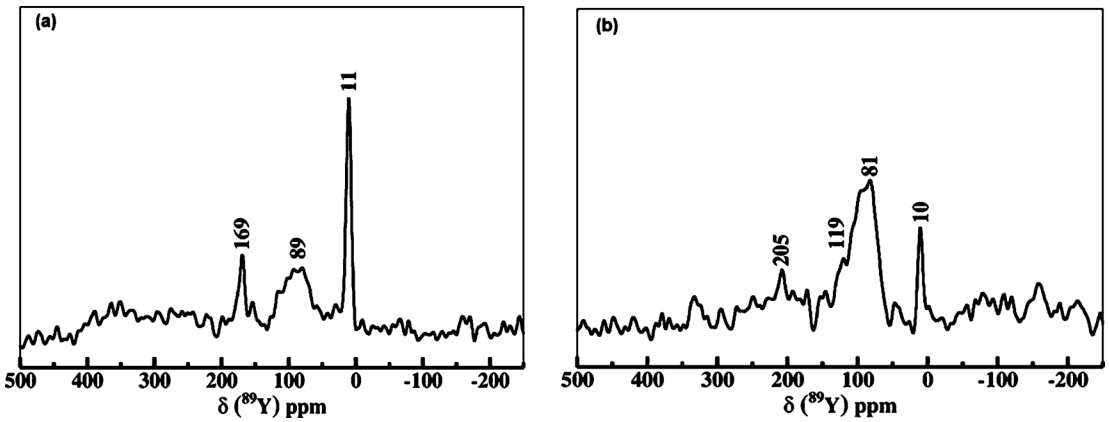

Fig. 8. (a) ^{89}Y MAS-NMR spectrum of (a) MYS/Cd and (b) MYS/Pb.

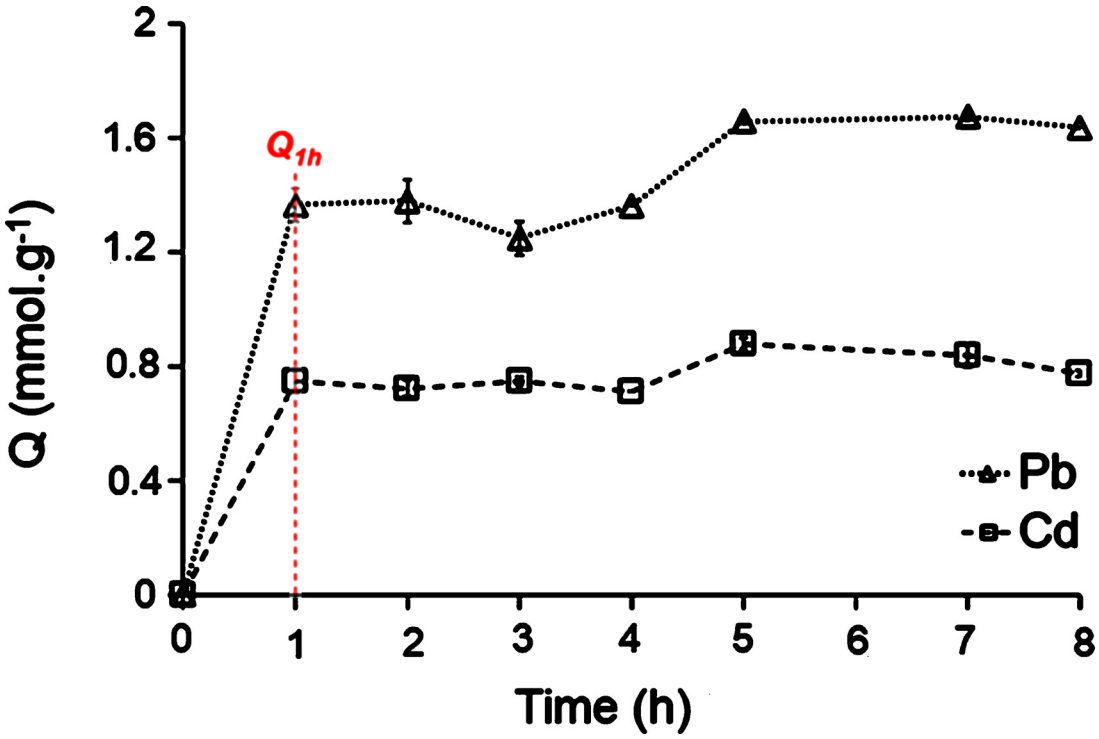

Fig. 9. Effect of the contact time on the adsorption of Pb^{2+} and Cd^{2+} onto MYS.

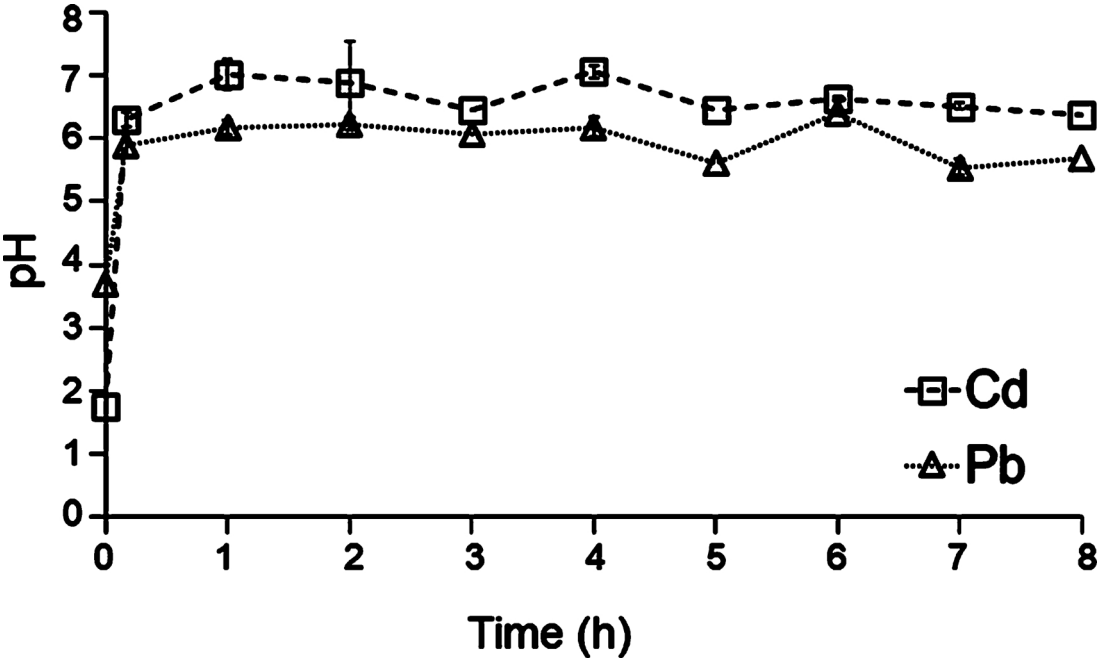

Fig. 10. Temporal profiles of pH during the adsorption experiments. The initial pH values of the prepared solutions were 1.74 ($CdCl_2$) and 3.70 ($PbNO_3)_2$. [$CdCl_2$ or $Pb(NO_3)_2$] = 0.05 mol L^{-1}; (□) cadmium; (△) lead.

coordination number decreases [43]. Therefore, these chemical shifts could be explained by the existence of yttrium species with greater coordination than the octahedral yttrium present in monteregianite, surrounded by seven or eight oxygen atoms in the structure. It is possible that sodium atoms were attached to the yttrium atoms by oxygen bonds, so consequently changes would be expected in the ^{89}Y MAS-NMR spectrum after ion exchange with cadmium and lead cations.

Fig. 8 shows the ^{89}Y MAS-NMR resonance spectra for the MYS/Cd and MYS/Pb samples. Chemical shifts at -169 ppm (MYS/Cd – Fig. 8a) and -205 ppm (MYS/Pb – Fig. 8b) were equivalent to those observed for the as-synthesized MYS (at -160 and -220 ppm – Fig. 7). The previous chemical shift located at around -89 ppm remained the same in the MYS/Cd spectrum and was slightly shifted to -81 ppm in the MYS/Pb spectrum, indicating that the main octahedral yttrium sites were still present in the crystal structure. However, two distinct chemical shifts appeared at -10 and -11 ppm, compared to the ^{89}Y MAS-NMR spectrum for the as-synthesized MYS material. Therefore, it could be concluded that lead and cadmium entered the sites previously occupied by sodium

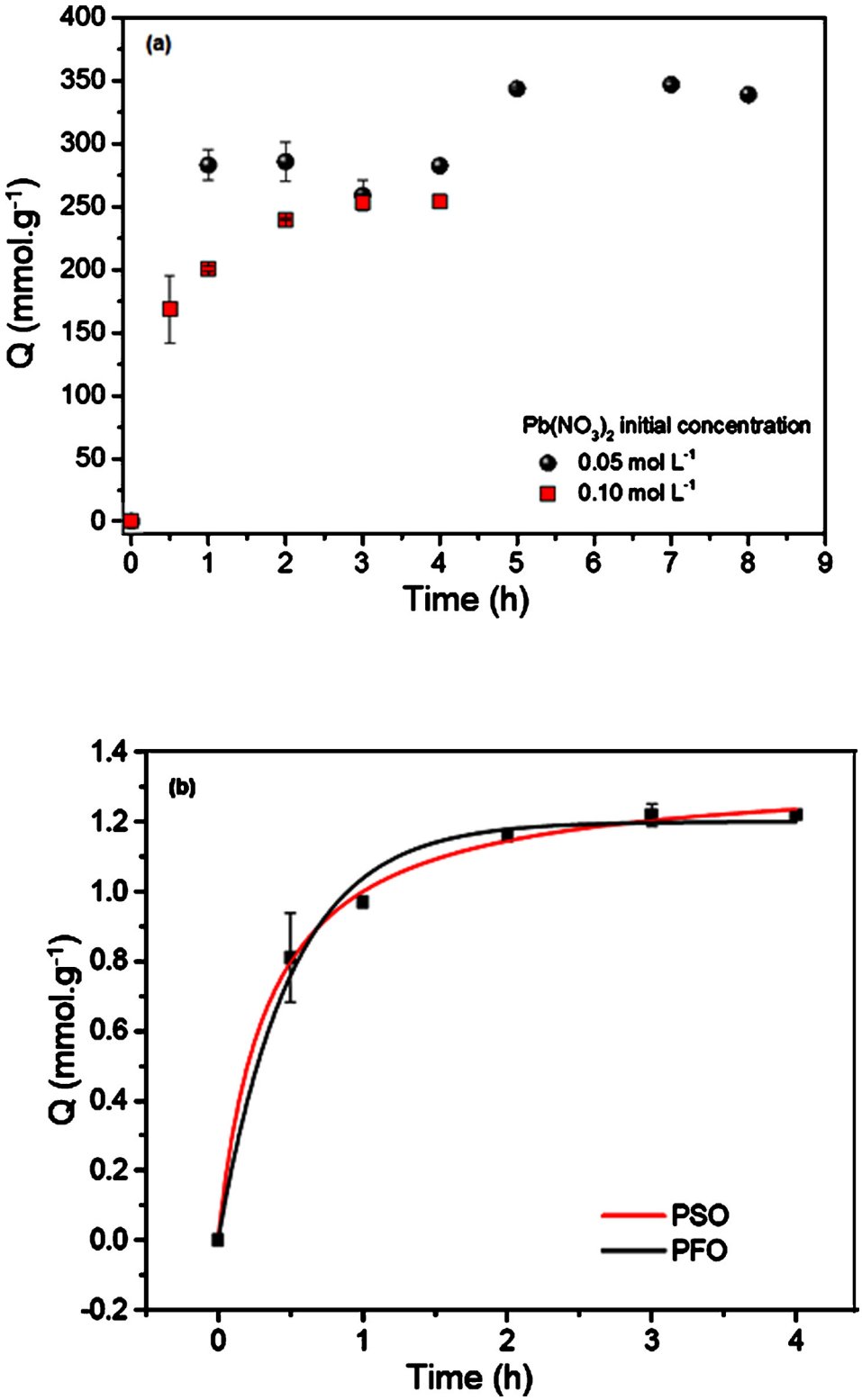

Fig. 11. (a) Comparison between Kinect essays using a [$Pb(NO_3)_2$] solution with initial concentration of 0.05 and 0.1 mol L^{-1} and (b) Experimental data and kinetic model fits for the adsorption of lead onto the metallo-yttrium silicate. [$Pb(NO_3)_2$] = 0.1 mol L^{-1}; black line: pseudo-first order (PFO) model; red line: pseudo-second order (PSO) model. All runs were performed in duplicate.

in the as-synthesized metallo-yttrium silicate structure, causing a significant change of the chemical environment around the yttrium nuclei.

The uptake amount (Q) of Pb^{2+} and Cd^{2+} ions by the MYS as a function of time (initial concentrations of both solutions = 0.05 mol L^{-1}) is shown in fig. 9. It is noted that the amount of the toxic metals uptake by MYS increases in function of time until reached the equilibrium. The first hour of Kinect essay (Q_{1h} – see Fig. 9) is crucial for the amount adsorbed of theses metal species, which demonstrated a fast and high Pb^{2+} (Q_{1h} = 1.37 mmol.g^{-1}) and for Cd^{2+} (Q_{1h} = 0.75 mmol.g^{-1}) removal from aqueous solution. The initial adsorption is probably due to the abundant availability of adsorption sites and the higher concentration gradient that drives diffusion of Pb^{2+} and

Table 2
Kinetic parameters of pseudo-first-order and pseudo-second-order models[a] for the adsorption of Pb^{2+} onto MYS.

Model	Parameter	Data
Pseudo-first order kinect model	k_1 (min^{-1})	2.0
	$Q_{eq,\ Pb,calc}$ ($mmol.\ g^{-1}$)	1.88
	R^2	0.9903
	χ^2_{red}	2.12×10^{-3}
	k_2 ($g.\ mg^{-1}.\ min^{-1}$)	2.2
Pseudo-second order kinect model	$Q_{eq,Pb,calc}$ ($mol.\ g^{-1}$)	2.10
	R^2	0.9980
	χ^2_{red}	4.41×10^{-4}

[a] $Q_{e,Pb,\ exp}$ ($mmol.\ g^{-1}$) and $Q_{e,Pb,\ calc}$ ($mmol.\ g^{-1}$) are the amounts of the metal ions adsorbed onto MYS at equilibrium for experimental and calculated and, k_1 ($L.\ min^{-1}$) and k_2 ($g.\ mg^{-1}.\ min^{-1}$) are the rate constants of the first and second order models, respectively.

Table 3
Previously reported maximum adsorption capacities of the various layered mineral adsorbents for Cd(II) and Pb(II) at room temperature.

Adsorption capacity ($mmol.\ g^{-1}$)			
Adsorbent	Cd	Pb	Ref
Phosphate rock	0.09	0.06	[45]
Vermiculite	0.12	0.12	[46]
Montmorillonite	0.28	0.15	[47]
Kaolinite	0.1	0.08	[48]
Turkish illitic clay	0.11	0.26	[49]
Metallo-yttrium silicate	0.77	1.63	This study

Cd^{2+} ions from solution to the surface of MYS. The removal percentage achieved by MYS reached 94 % and 74 %, respectively for Pb(II) and Cd (II) using 0,5 g of the adsorbent. Adsorbates–adsorbent interactions reached equilibrium within 5 h (MYS/Pb) and 1 h (MYS/Cd). These results demonstrated that the MYS could be applied as a promising material for environmental pollution management i.e. efficient adsorbent for removal of toxic metals from aqueous solution.

Fig. 10 shows the temporal evolution of the pH during the adsorption experiments with initial salt concentrations of 0.05 mol L^{-1}. The pH values changed substantially after mixing the salt solutions with the MYS, from 1.74 to 6.31 for Cd^{2+}, and from 3.70 to 5.90 for Pb^{2+}. No further significant changes of pH were observed in function of time, irrespective of the metal evaluated. For Cd^{2+}, a maximum pH difference of 6.47 ± 0.66 was obtained in 3 h, providing a good indication that the adsorption process was stable. Note that several adsorption experiments with cadmium solution (0.05 $mol.L^{-1}$) have clearly indicated that the equilibrium was quickly reached, therefore indicating no clear trend throughout the experiments, i.e.: $Q_{1h} \approx Q_{8h}$ (Fig. 9). On the other hand, the preliminary experiments with lead were more promising in terms of sorption capacity ($Q_{Pb,\ max}$ = 1.67 $mmol.\ g^{-1}$ versus $Q_{Cd,\ max}$ = 0.88 $mmol.g^{-1}$; $[Pb]_0$ and $[Cd]_0$ = 0.05 $mol.L^{-1}$) compared to cadmium. Therefore, adsorption experiments with a higher concentration of lead solution (0.10 $mol.L^{-1}$) were carried out, and a clear trend was revealed, as well as the experimental data were well fitted and the kinetics modeled (Fig.11). Regarding the data set obtained for cadmium, the kinetic modeling was not feasible.

Fig. 11 shows the adsorption of Pb^{2+} onto MYS and the curves fitted to the experimental data (plots of *qt* versus *t*) using the pseudo-first order (PFO) and pseudo-second-order (PSO) Kinect models. Initially, the rapid interaction of MYS and toxic metals is probably due to the rich availability of adsorption sites of the MYS which create an osmotic transport which are associated to the diffusion of Pb^{2+} ions from solution to the surface of the material. Over the course of time, the unoccupied vacant sites were expected to be more difficult to fill, due to limitation of available sites of MYS for occupation and the electrostatic repulsion between adsorbed Pb^{2+} ions and incoming Pb^{2+} ions. Consequently, the adsorption rate decreased until reaching the equilibrium stage. As expected, a higher initial Pb^{2+} concentration resulted in lower metal removal (43 %, compared to 94 %). On the other hand, equilibrium was reached more rapidly using a $Pb(NO_3)_2$ with an initial concentration of 0.1 mol L^{-1} (see Fig. 11a). There was no significant change of the pH and the adsorption process was very stable during in function of time. The pseudo-first order and pseudo-second order models were used to evaluate the lead adsorption kinetics. The parameter data and predicted values are listed in Table 2.

The PFO and PSO models provided high R^2 values of 0.9903 and 0.9980, respectively. The adsorption of Pb^{2+} (with $[Pb(NO_3)_2]_0$ = 0.1 $mol.L^{-1}$) reached equilibrium after 180 min, which was longer than the time of 60 min reported previously for the adsorption of Pb^{2+} on the ETS-10 titanosilicate [44]. The PSO kinetic model provided higher R^2, lower χ^2_{red} (2.2×10^{-3}) and the $Q_{eq,Pb,\ calc}$ values estimated to the $Q_{eq,Pb,\ exp}$ values (1.63 $mmol.g^{-1}$). A higher $Q_{eq,Pb,\ calc}$ value (1.88 $mg.g^{-1}$) was estimated by the PFO model. According to Ho and McKay [32], a good fit for the pseudo-second order model suggests that the rate-limiting step in an adsorption process is attributed to chemisorption. The model results were in agreement with the physicochemical characterizations performed in this work, demonstrating the sharing or exchange of electrons between MYS and Pb^{2+} ions in aqueous solution. The adsorption capacities of Pb^{2+} and Cd^{2+} onto various layered materials, collected from the references [45–49] are listed in Table 3 and the comparative results show that the adsorption capacities of the novel MYS is greater than those reported previously.

4. Conclusions

A new metallosilicate based on yttrium was synthesized and fully characterized by XRD, FT-IR, ^{29}Si MAS-NMR, and ^{89}Y MAS-NMR. The mixed framework of the material was confirmed by the distinct groups of chemical shifts observed in the ^{29}Si MAS-NMR spectrum (at -82 to -87 ppm, -91 to -94 ppm, -96 to -102 ppm, and -105 to -108 ppm) and four chemical shifts (at -89, -142, -160, and -220 ppm) observed in the ^{89}Y MAS-NMR spectrum. The results of adsorption and kinetic assays demonstrated the potential of the yttrium silicate for the removal of cadmium and lead from solution. For lead, dynamic equilibrium was reached after five hours, with removal of 94 % of the lead, while for cadmium, equilibrium was achieved in the first hour and 74 % of the cadmium was removed. The adsorption behavior was modeled using the pseudo-first order (PFO) and pseudo-second order (PSO) kinetic models. Both PFO and PSO models provided high R^2 values (0.9903 and 0.9980, respectively), while lower χ^2_{red} was obtained for the PSO model. However, the estimated $Q_{eq\ calc}$ value obtained with the PFO model was equal to the experimental $Q_{eq\ exp}$ value, whereas $Q_{eq\ calc}$ estimated by the PSO model was higher. The findings of this study indicated that the MYS is stable and has the potential to be applied in the treatment of aqueous solutions containing toxic metals.

CRediT authorship contribution statement

Vinicius Litrenta Medeiros: Investigation, Methodology, Resources. **Leandro Goulart de Araujo:** Investigation, Methodology. **Davi Rubinho Ratero:** Investigation. **Alex Silva Paula:** Investigation. **Eduardo Ferreira Molina:** Resources, Formal analysis. **Christian Jaeger:** Resources, Methodology. **Júlio Takehiro Marumo:** Investigation. **José Geraldo Nery:** Investigation, Methodology, Funding acquisition.

Declaration of Competing Interest

The authors declare that they have no known competing financial interests or personal relationships that could have appeared to

influence the work reported in this paper.

Acknowledgments

Financial support for this research project was provided by the São Paulo State Research Foundation (FAPESP), in the form of a scientific award to J.G.N. (grants #11/51851-5 and #19/01858-5), and by National Council for Scientific and Technological Development (CNPq) (grants #465594/2014-0 and #406761/2013-2). The authors also thank Nuclear and Energy Research Institute (IPEN) for financial support.

References

[1] J.O. Nriagu, A silent epidemic of environmental metal poisoning? Environ. Pollut. 50 (1988) 139–161, https://doi.org/10.1016/0269-7491(88)90189-3.
[2] M.A.S. Laidlaw, G.M. Filippelli, Resuspension of urban soils as a persistent source of lead poisoning in children: a review and new directions, Appl. Geochem. 23 (2008) 2021–2039, https://doi.org/10.1016/j.apgeochem.2008.05.009.
[3] D.C. Adriano, Trace Elements in the Terrestrial Environment, Springer Science & Business Media, 2013.
[4] H. Morgan, G.A. Smart, J.C. Sherlock, The Shipham report. An investigation into cadmium contamination and its implications for human health. Intakes of metal, Sci. Total Environ. 75 (1988) 71–100, https://doi.org/10.1016/0048-9697(88)90160-x.
[5] B.J. Alloway, Sources of heavy metals and metalloids in soils, in: B.J. Alloway (Ed.), Heavy Metals in Soils: Trace Metals and Metalloids in Soils and Their Bioavailability, Springer, Dordrecht, Netherlands, 2013, pp. 11–50, , https://doi.org/10.1007/978-94-007-4470-7_2.
[6] A.A. Juwarkar, A. Nair, K.V. Dubey, S.K. Singh, S. Devotta, Biosurfactant technology for remediation of cadmium and lead contaminated soils, Chemosphere. 68 (2007) 1996–2002, https://doi.org/10.1016/j.chemosphere.2007.02.027.
[7] S.K.R. Yadanaparthi, D. Graybill, R. von Wandruszka, Adsorbents for the removal of arsenic, cadmium, and lead from contaminated waters, J. Hazard. Mater. 171 (2009) 1–15, https://doi.org/10.1016/j.jhazmat.2009.05.103.
[8] H. Cho, D. Oh, K. Kim, A study on removal characteristics of heavy metals from aqueous solution by fly ash, J. Hazard. Mater. 127 (2005) 187–195, https://doi.org/10.1016/j.jhazmat.2005.07.019.
[9] V.K. Gupta, S. Agarwal, T.A. Saleh, Synthesis and characterization of alumina-coated carbon nanotubes and their application for lead removal, J. Hazard. Mater. 185 (2011) 17–23, https://doi.org/10.1016/j.jhazmat.2010.08.053.
[10] M.W. Amer, F.I. Khalili, A.M. Awwad, Adsorption of lead, zinc and cadmium ions on polyphosphate-modified kaolinite clay, J. Environ. Chem. Ecotoxicol. 2 (2009) 1–8.
[11] M.W. Yap, N.M. Mubarak, J.N. Sahu, E.C. Abdullah, Microwave induced synthesis of magnetic biochar from agricultural biomass for removal of lead and cadmium from wastewater, J. Ind. Eng. Chem. 45 (2017) 287–295, https://doi.org/10.1016/j.jiec.2016.09.036.
[12] M. Vaclavikova, P. Misaelides, G. Gallios, S. Jakabsky, S. Hredzak, Removal of cadmium, zinc, copper and lead by red mud, an iron oxides containing hydrometallurgical waste, Studies in Surface Science and Catalysis, Elsevier, 2005, pp. 517–525, https://doi.org/10.1016/S0167-2991(05)80179-X.
[13] T. Halttunen, S. Salminen, R. Tahvonen, Rapid removal of lead and cadmium from water by specific lactic acid bacteria, Int. J. Food Microbiol. 114 (2007) 30–35, https://doi.org/10.1016/j.ijfoodmicro.2006.10.040.
[14] R. Vimala, N. Das, Biosorption of cadmium (II) and lead (II) from aqueous solutions using mushrooms: a comparative study, J. Hazard. Mater. 168 (2009) 376–382, https://doi.org/10.1016/j.jhazmat.2009.02.062.
[15] W. Shi, H. Shao, H. Li, M. Shao, S. Du, Progress in the remediation of hazardous heavy metal-polluted soils by natural zeolite, J. Hazard. Mater. 170 (2009) 1–6, https://doi.org/10.1016/j.jhazmat.2009.04.097.
[16] P. Misaelides, Application of natural zeolites in environmental remediation: a short review, Microporous Mesoporous Mater. 144 (2011) 15–18, https://doi.org/10.1016/j.micromeso.2011.03.024.
[17] C.S. Cundy, P.A. Cox, The hydrothermal synthesis of zeolites: history and development from the earliest days to the present time, Chem. Rev. 103 (2003) 663–702, https://doi.org/10.1021/cr020060i.
[18] C.S. Cundy, P.A. Cox, The hydrothermal synthesis of zeolites: precursors, intermediates and reaction mechanism, Microporous Mesoporous Mater. 82 (2005) 1–78, https://doi.org/10.1016/j.micromeso.2005.02.016.
[19] M. Panayotova, B. Velikov, Kinetics of heavy metal ions removal by use of Natural Zeolite, J. Environ. Sci. Health, Part A. 37 (2002) 139–147, https://doi.org/10.1081/ESE-120002578.
[20] M. Delkash, B. Ebrazi Bakhshayesh, H. Kazemian, Using zeolitic adsorbents to cleanup special wastewater streams: a review, Microporous Mesoporous Mater. 214 (2015) 224–241, https://doi.org/10.1016/j.micromeso.2015.04.039.
[21] J. Rocha, M.W. Anderson, Microporous titanosilicates and other novel mixed octahedral-tetrahedral framework oxides, Eur. J. Inorg. Chem. 18 (2000) https://doi.org/143421948/00/050520801.
[22] J. Rocha, P. Ferreira, Z. Lin, P. Brandão, A. Ferreira, J.D. Pedrosa de Jesus, Synthesis and structural characterization of microporous yttrium and calcium silicates, J. Phys. Chem. B 102 (1998) 4739–4744, https://doi.org/10.1021/jp9803337.
[23] Y.D. Noh, S. Komarneni, Mercury(II) exchange by highly charged swelling micas, sodium engelhard Titanosilicate-4, and sodium titanosilicate, Environ. Sci. Technol. 45 (2011) 6954–6960, https://doi.org/10.1021/es200712r.
[24] L.D. Barreira, P.F. Lito, B.M. Antunes, M. Otero, Z. Lin, J. Rocha, E. Pereira, A.C. Duarte, C.M. Silva, Effect of pH on cadmium (II) removal from aqueous solution using titanosilicate ETS-4, Chem. Eng. J. 155 (2009) 728–735, https://doi.org/10.1016/j.cej.2009.09.014.
[25] C.C. Pavel, K. Popa, Investigations on the ion exchange process of Cs+ and Sr2+ cations by ETS materials, Chem. Eng. J. 245 (2014) 288–294, https://doi.org/10.1016/j.cej.2014.02.036.
[26] I.V. Pekov, Microporous framework silicate minerals with rare and transition elements: minerogenetic aspects, Rev. Mineral. Geochem. 57 (2005) 145–171, https://doi.org/10.2138/rmg.2005.57.5.
[27] D.Y. Pushcharovskii, I.V. Pekov, M. Pasero, E.R. Gobechiya, S. Merlino, N.V. Zubkova, Crystal structure of cation-deficient calciohilairite and possible mechanisms of decationization in mixed-framework minerals, Crystallogr. Rep. 47 (2002) 748–752.
[28] P.K. Subrata Ghose, Charles F. Sen Gupta, Campana, Symmetry and crystal structure of montregianite, Na4K2Y2Si16O38. 10H2O, a double-sheet silicate with zeolitic properties, Am. Mineral. 72 (1987) 365–374.
[29] M. Wierzbicka-Wieczorek, U. Kolitsch, E. Tillmanns, Novel synthetic alkali-yttrium silicates with a new microporous mixed framework topology: (Rb,Cs) $_9$ Y $_7$ Si $_{24}$ O $_{63}$ and isotypic Rb $_9$ Y $_7$ Si $_{24}$ O $_{63}$, Cryst. Res. Technol. 43 (2008) 1210–1219, https://doi.org/10.1002/crat.200800325.
[30] U. Kolitsch, M. Wierzbicka-Wieczorek, E. Tillmanns, Crystal Chemistry and Topology of TWO FLUX-GROWN yttrium silicates, BaKYSi2O7 and Cs3YSi8O19, Can. Mineral. 47 (2009) 421–431, https://doi.org/10.3749/canmin.47.2.421.
[31] S. Azizian, Kinetic models of sorption: a theoretical analysis, J. Colloid Interface Sci. 276 (2004) 47–52, https://doi.org/10.1016/j.jcis.2004.03.048.
[32] Y.S. Ho, G. McKay, Pseudo-second order model for sorption processes, Process. Biochem. 34 (1999) 451–465, https://doi.org/10.1016/S0032-9592(98)00112-5.
[33] R.A. Fideles, G.M.D. Ferreira, F.S. Teodoro, O.F.H. Adarme, L.H.M. da Silva, L.F. Gil, L.V.A. Gurgel, Trimellitated sugarcane bagasse: A versatile adsorbent for removal of cationic dyes from aqueous solution. Part I: Batch adsorption in a monocomponent system, J. Colloid Interface Sci. 515 (2018) 172–188, https://doi.org/10.1016/j.jcis.2018.01.025.
[34] A. Altomare, C. Giacovazzo, A. Guagliardi, A.G.G. Moliterni, R. Rizzi, P.-E. Werner, New techniques for indexing: N-TREOR in EXPO, J. Appl. Crystallogr. 33 (2000) 1180–1186, https://doi.org/10.1107/S0021889800006427.
[35] I. Persson, K. Lyczko, D. Lundberg, L. Eriksson, A. Płaczek, Coordination chemistry study of hydrated and solvated lead(II) ions in solution and solid state, Inorg. Chem. 50 (2011) 1058–1072, https://doi.org/10.1021/ic1017714.
[36] C. Ronay, K. Seff, Lead oxide hydroxide clusters in Pb9O(OH)4-A, zeolite A exchanged with Pb2+ at Ph 6.0, Zeolites. 13 (1993) 97–101, https://doi.org/10.1016/0144-2449(93)90067-D.
[37] W. Shibata, K. Seff, Pb2 Exchange Isotherms for Zeolite Na-X at pH 5, 6, and 7, Zeolites 19 (1997) 87–89, https://doi.org/10.1016/S0144-2449(97)00053-5.
[38] C. Ronay, K. Seff, Crystal structures of lead (Pb6)-A and lead hydroxide hydrate (Pb9(OH)8(H2O)3-A. Zeolite A ion exchanged with lead(2+) at pH 4.3 and 6.0 and evacuated, J. Phys. Chem. 89 (1985) 1965–1970, https://doi.org/10.1021/j100256a030.
[39] T. Sun, K. Seff, Pulsed-neutron powder-diffraction study of lead sulfide and deuterium ions in zeolite Y, J. Phys. Chem. 97 (1993) 7719–7723, https://doi.org/10.1021/j100131a048.
[40] G. Engelhardt, D. Michel, High-resolution Solid-state NMR of Silicates and Zeolites, (1987) (accessed October 16, 2019), https://www.osti.gov/biblio/6743230.
[41] P.S. Singh, T. Bastow, M. Trigg, Structural studies of geopolymers by 29Si and 27Al MAS-NMR, J. Mater. Sci. 40 (2005) 3951–3961, https://doi.org/10.1007/s10853-005-1915-x.
[42] K. Kawata, H. Maekawa, T. Nemoto, T. Yamamura, Local structure analysis of YSZ by Y-89 MAS-NMR, Solid State Ion. 177 (2006) 1687–1690, https://doi.org/10.1016/j.ssi.2006.02.030.
[43] N. Kim, J.F. Stebbins, Vacancy and cation distribution in yttria-doped Ceria: an ^{89} Y and ^{17} O MAS NMR study, Chem. Mater. 19 (2007) 5742–5747, https://doi.org/10.1021/cm0715388.
[44] L. Lv, M.P. Hor, F. Su, X.S. Zhao, Competitive adsorption of Pb2+, Cu2+, and Cd2+ ions on microporous titanosilicate ETS-10, J. Colloid Interface Sci. 287 (2005) 178–184, https://doi.org/10.1016/j.jcis.2005.01.073.
[45] Z. Elouear, J. Bouzid, N. Boujelben, M. Feki, F. Jamoussi, A. Montiel, Heavy metal removal from aqueous solutions by activated phosphate rock, J. Hazard. Mater. 156 (2008) 412–420, https://doi.org/10.1016/j.jhazmat.2007.12.036.
[46] G. Abate, J.C. Masini, Influence of pH, ionic strength and humic acid on adsorption of Cd(II) and Pb(II) onto vermiculite, Colloids Surf. A Physicochem. Eng. Asp. 262 (2005) 33–39, https://doi.org/10.1016/j.colsurfa.2005.04.005.
[47] S. Sen Gupta, K.G. Bhattacharyya, Immobilization of Pb(II), Cd(II) and Ni(II) ions on kaolinite and montmorillonite surfaces from aqueous medium, J. Environ. Manage. 87 (2008) 46–58, https://doi.org/10.1016/j.jenvman.2007.01.048.
[48] K.O. Adebowale, I.E. Unuabonah, B.I. Olu-Owolabi, The effect of some operating variables on the adsorption of lead and cadmium ions on kaolinite clay, J. Hazard. Mater. 134 (2006) 130–139, https://doi.org/10.1016/j.jhazmat.2005.10.056.
[49] D. Ozdes, C. Duran, H.B. Senturk, Adsorptive removal of Cd(II) and Pb(II) ions from aqueous solutions by using Turkish illitic clay, J. Environ. Manage. 92 (2011) 3082–3090, https://doi.org/10.1016/j.jenvman.2011.07.022.